Ecosystem processes at the watershed scale: Hydrologic vegetation gradient as an indicator for lateral hydrologic connectivity of headwater catchments

Taehee Hwang,[1] Lawrence E. Band,[1,2] James M. Vose,[3] and Christina Tague[4]

Received 19 August 2011; revised 30 April 2012; accepted 2 May 2012; published 13 June 2012.

[1] Lateral water flow in catchments can produce important patterns in water and nutrient fluxes and stores and also influences the long-term spatial development of forest ecosystems. Specifically, patterns of vegetation type and density along hydrologic flow paths can represent a signal of the redistribution of water and nitrogen mediated by lateral hydrologic flow. This study explores the use of emergent vegetation patterns to infer ecohydrologic processes and feedbacks in forested headwater catchments. We suggest a hydrologic gradient of vegetation density as an indicator of lateral connectivity within headwater catchments. We define the hydrologic vegetation gradient (HVG) as the increase of normalized difference vegetation index per unit increase of the topographic wetness index. HVG are estimated in different headwater catchments in the Coweeta Hydrologic Laboratory using summer IKONOS imagery. We use recession slope analysis with gauge data and a distributed ecohydrological model to characterize the patterns of seasonal flow regimes within the catchments. Correlations between HVG, catchment runoff, early recession parameters, and model parameters show the interactive role of vegetation and lateral hydrologic connectivity of systems in addition to climatic and geomorphic controls. This suggests that HVG effectively represents the level of partitioning between localized water use and lateral water flow along hydrologic flow paths, especially during the growing season. It also presents the potential to use simple remotely sensed hydrologic vegetation gradients as an indicator of lateral hydrologic connectivity to extrapolate recession behavior and key model parameters of distributed hydrological models for ungauged headwater catchments.

Citation: Hwang, T., L. E. Band, J. M. Vose, and C. Tague (2012), Ecosystem processes at the watershed scale: Hydrologic vegetation gradient as an indicator for lateral hydrologic connectivity of headwater catchments, *Water Resour. Res.*, *48*, W06514, doi:10.1029/2011WR011301.

1. Introduction

[2] Hydrologic connectivity has emerged as a central concept in hillslope hydrology. Hydrologic connectivity has been studied as a function of climate forcing (e.g., precipitation pattern), antecedent soil moisture conditions, dominant flow regimes, and physical properties of watersheds including surface/subsurface topography, soil, and geological properties [e.g., *Detty and McGuire*, 2010; *Hopp and McDonnell*, 2009; *Ali and Roy*, 2010]. Effective connectivity is strongly linked to runoff generation dynamics and soil moisture organization within catchments [e.g., *James and Roulet*, 2007; *Jencso et al.*, 2009; *Western et al.*, 2001]. Hydrologic connectivity is usually defined from both flow path continuity between uplands, riparian zones, and stream channels [e.g., *Jencso et al.*, 2009] and connectivity metrics from surface soil moisture measurements [e.g., *Western et al.*, 2001]. *Ali and Roy* [2010] pointed that these definitions are not contradictory as soil moisture patterns are typically a function of dominant subsurface flow processes.

[3] Hydrologic connectivity has also been regarded as a key concept for understanding ecological connectivity of terrestrial and aquatic ecosystems through lateral transport of water or nutrients [*Pringle*, 2003; *Bracken and Croke*, 2007; *Tetzlaff et al.*, 2010]. For example, vegetation often represents lateral redistribution of water and nutrients at the hillslope scale. Forest vegetation also increases infiltration rates and water holding capacity of soils by increasing macroporosity and organic matter, resulting in greater hydraulic conductivity and lower bulk density [e.g., *Price et al.*, 2010]. Therefore, subsurface and saturated overland flow usually dominates forested watersheds during wet periods and effectively drains saturated and near saturated conditions. During

[1]Institute for the Environment, University of North Carolina at Chapel Hill, Chapel Hill, North Carolina, USA.
[2]Department of Geography, University of North Carolina at Chapel Hill, Chapel Hill, North Carolina, USA.
[3]Coweeta Hydrologic Laboratory, Forest Service, USDA, Otto, North Carolina, USA.
[4]Bren School of Environmental Science and Management, University of California at Santa Barbara, Santa Barbara, California, USA.

Corresponding author: T. Hwang, Institute for the Environment, University of North Carolina at Chapel Hill, Campus Box 1105, Chapel Hill, NC 27599-1105, USA. (h7666@email.unc.edu)

0043-1397/12/2011WR011301

the growing season, vegetation consumes water through interception and transpiration, retaining water for ecosystem use and decreasing lateral hydrologic flux. Many studies have reported strong seasonal patterns of hydrologic connectivity primarily driven by vegetation in temperate subhumid or humid catchments [*Detty and McGuire*, 2010; *Western et al.*, 2001; *Grayson et al.*, 1997].

[4] An interactive role of vegetation on lateral hydrologic flows has been extensively examined in semiarid ecosystems (e.g., "tiger bush" [*Ludwig et al.*, 2005]), where hydrologic connectivity is disrupted by local water and nutrient sinks provided by isolated bands of vegetation, and runoff is rarely connected to local streams. In humid or subhumid temperate forests, soil water is also an important structuring element of forest community and biodiversity [*Day et al.*, 1988]. In steep forested headwater catchments, shallow subsurface flow is a main source of sustained base flow [*Hewlett and Hibbert*, 1967]. Therefore, spatial patterns of vegetation within these catchments are tightly coupled with the degree of dependence on multiple resources (water or nutrients) mediated by lateral hydrologic flows [*Hwang et al.*, 2009]. *Mackay and Band* [1997] pointed out that the covariance of leaf area index with wetness intervals is related to a limiting factor along hydrologic flow paths. Several sap-flux studies also suggest dominant topographic and edaphic controls on spatial heterogeneity of transpiration through soil moisture dynamics [*Mackay et al.*, 2010; *Ford et al.*, 2007; *Eberbach and Burrows*, 2006]. In this sense, emergent vegetation patterns along hydrologic flow paths are important indicators for both local-scale water partitioning and hillslope-scale lateral redistribution of soil water [see *Thompson et al.*, 2011].

[5] Hydrologic responses of a catchment are usually related to topographic controls on hydrological processes. Major parameters of lumped hydrologic models are often estimated in a statistical manner to transfer dominant hydrologic behavior to ungauged catchments [e.g., *Kokkonen et al.*, 2003; *Wagener and Wheater*, 2006]. In addition, observed hydrologic response (e.g., mean residence time) is also explained by topographic characteristics of a catchment, such as flow path length, flow path gradient, upslope area, and aspect [*McGuire et al.*, 2005; *Tetzlaff et al.*, 2009; *Broxton et al.*, 2009]. However, the importance of vegetation and its interactive role with lateral water redistribution has often been disregarded despite significant influence of antecedent soil moisture conditions, and resulting nonlinear hydrologic runoff and recharge response [*Detty and McGuire*, 2010; *McGuire and McDonnell*, 2010].

[6] Vegetation productivity is tightly coupled with long-term vegetation water use [e.g., *Webb et al.*, 1978; *Law et al.*, 2002] via gas exchange processes through leaf stomata. However, few studies have related catchment-scale hydrologic behavior with vegetation dynamics. Recently, *Troch et al.* [2009] revisited the Horton index, originally suggested by *Horton* [1933], which describes the fraction of evapotranspiration to catchment wetting. *Brooks et al.* [2011] and *Voepel et al.* [2011] have effectively shown how remotely sensed vegetation (e.g., normalized difference vegetation index) is related to long-term catchment-scale hydrologic partitioning across different climate regions.

[7] This study examines the coevolution of forest patterns with hydrologic landscapes, and specifically along lateral hydrologic flow paths in headwater catchments. We assume that vegetation patterns effectively represent not only long-term carbon uptake (photosynthesis) but also concurrent vegetation water use (evapotranspiration) at given topoclimatic settings. We use a simple indicator for hydrologic connectivity of the watershed system derived from remotely sensed vegetation, the hydrologic vegetation gradient (HVG). The interaction of the HVG with a set of hydrological measurements is investigated, including seasonal patterns of runoff production, recession coefficients, and behavioral parameter ranges for a distributed hydrological model in addition to topoclimatic and geomorphic factors. HVG is also investigated as a method to estimate early recession behavior and key model parameters without hydrologic observations. The objectives of this study are (1) to define and estimate the hydrologic vegetation gradient in headwater catchments from fine-resolution remote sensing imagery, (2) to relate HVG with annual hydrologic metrics, recession coefficients, and behavioral model parameter ranges from observed streamflow signals, and (3) to find dominant topographic controls on ecohydrologic connectivity in different headwater catchments.

2. Methods and Materials

2.1. Site Description

[8] The Coweeta Hydrologic Laboratory is located in western North Carolina, and is dominated by mixed hardwood Forests (Figure 1). The climate is classified as marine, humid temperate with precipitation evenly distributed throughout the year. Mean annual precipitation ranges from 1870 to 2500 mm with about a 5% increase for each 100 m elevation increase (Figure 2) [*Swift et al.*, 1988]. About two percent of total precipitation is snow [*Post et al.*, 1998]. Average annual streamflow ranges from 48% to 75% of precipitation in different headwater catchments [*Swift et al.*, 1988]. In spite of plentiful precipitation, soil moisture is an important structuring element of vegetation species [*Day et al.*, 1988] and density [*Bolstad et al.*, 2001]. Seasonal drought (late growing season) is also a key factor for forest competition and diversity [*Clark et al.*, 2011] due to topographically driven drainage and interannual hydroclimate variability (Figure 2). *Yeakley et al.* [1998] also showed that topography exerts the dominant control over hillslope-scale soil moisture patterns during dry seasons in the study site.

[9] The dominant vegetation species are oaks and mixed hardwoods including *Quercus* spp. (oaks), *Carya* spp. (hickory), *Nyssa sylvatica* (black gum), *Liriodendron tulipifera* (yellow poplar), and *Tsuga canadensis* (eastern hemlock), while major evergreen understory species are *Rhododendron maximum* (rhododendron) and *Kalmia latifolia* (mountain laurel) [*Day et al.*, 1988]. Soils are described as sandy loam inceptisols and ultisols, typically of colluvial origin. Bedrock is typically folded schist and gneiss [*Hales et al.*, 2009]. The diverse spatiotemporal vegetation dynamics in the Coweeta basin have been attributed to combined effects of complex terrain, consequent microclimate variation, disturbance history, and hydrological processes [*Ford et al.*, 2007; *Whittaker*, 1956; *Day and Monk*, 1974; *Hwang et al.*, 2011] and provide a unique opportunity to relate

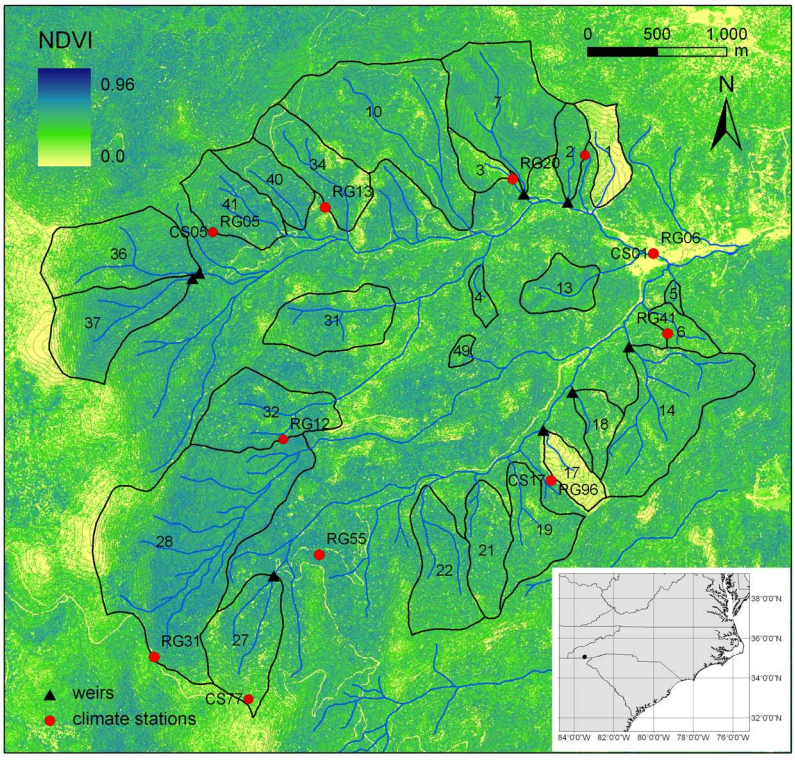

Figure 1. A study site (Coweeta Hydrologic Laboratory). Black and blue lines represent the watershed boundaries and streams. Numbers represent watershed ID, and contours are drawn at 20 m intervals. NDVI, normalized difference vegetation index; RG, rain gauge; CS, climate station.

different levels of lateral hydrologic connectivity with vegetation patterns in headwater catchments.

[10] Daily streamflow data from eight gauged headwater catchments are used in this study, five of which are located in lower-elevation regions (<900 m) and three in higher-elevation regions (>1250 m) (Figure 1 and Table 1). Several headwater catchments in Coweeta have a range of disturbance histories (Table 1). We limit our research to catchments where disturbance occurred at least 30 years ago. Details of the disturbance histories are available in Coweeta Long Term Ecological Research (LTER) homepage (http://coweeta.uga.edu/sitehistory).

2.2. Topographic Characteristics and Hydrologic Vegetation Gradient

[11] All topographic variables of headwater catchments (Table 1) are based on digital terrain analysis of light detection and ranging (LiDAR) elevation data. These data have about 6.1 m (20 ft) horizontal resolution with about 25 cm of root mean square errors. Aspect is transformed into a number ranging from −1 (northeast facing) to 1 (southwest facing) to create a more direct measure of radiation load for statistical analysis [*Beers et al.*, 1966]. Topographic wetness index (TI) [*Beven and Kirkby*, 1979] is calculated using the *D*-infinity method with flow proportioned between two downslope pixels according to gradient [*Tarboton*, 1997].

[12] The structure of vegetation patterns within headwater catchments is estimated from normalized difference vegetation index (NDVI) of a summer IKONOS image (1 June 2003; 4 m spatial resolution; Figure 1):

$$NDVI = (\rho_{NIR} - \rho_{RED})/(\rho_{NIR} + \rho_{RED}) \quad (1)$$

where ρ_{RED} and ρ_{NIR} are surface reflectance of red and near-infrared bands. NDVI is calculated at the same horizontal resolution as other topographic variables (6.1 m) by resampling reflectance. The hydrologic vegetation gradient is defined as the average increase of NDVI with a unit increase of TI in this study (dNDVI/dTI) within a headwater catchment, calculated by a linear regression of average NDVI values from binned groups at equal TI intervals (0.5). Only groups with more than 15 pixels are considered in this calculation. HVG is designed to represent only the hillslope-scale vegetation gradients by excluding long tails in TI distributions which generally represent streams. This simple linear estimate captures first-order hillslope-scale changes in vegetation density, although more detailed descriptors of canopy pattern may yield additional insight.

[13] NDVI is typically log linearly correlated to leaf area index (LAI) [*Asrar et al.*, 1984; *Sellers*, 1985], a measure of foliar density. LAI is usually defined as half total leaf area per unit ground area [*Chen and Black*, 1992], and largely determines canopy interception capacity for evaporation and potential transpiration through stomata. There are several reasons to compute the HVG with NDVI rather than LAI. First, NDVI is widely used remote sensing and more generally available than LAI. Second, NDVI has a linear

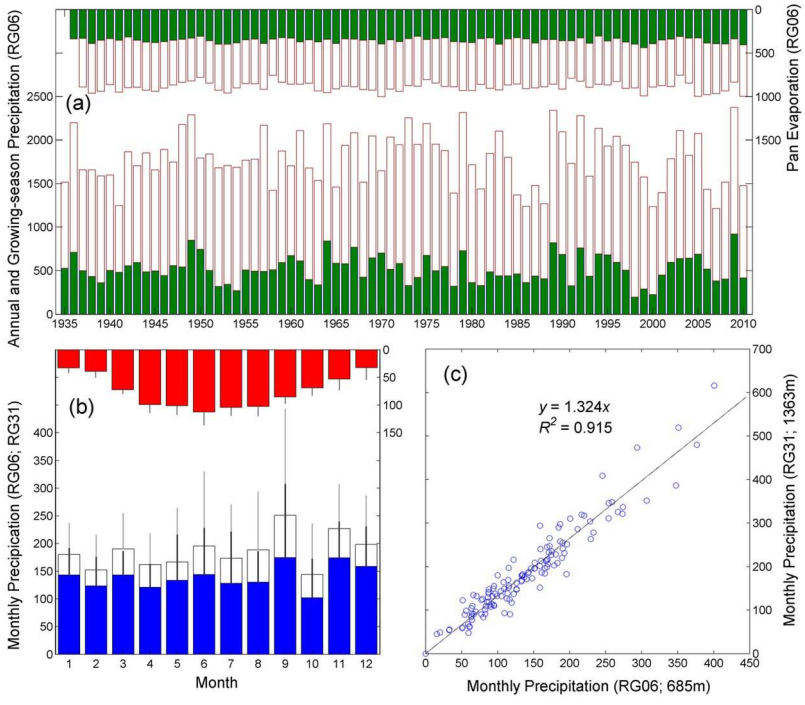

Figure 2. (a) Annual (white bars) and late growing season (July–October; green bars) precipitation and pan evaporation (reverse *y* axis) patterns at the base climate station (RG06; elevation 685 m). (b) Monthly mean precipitation and pan evaporation (reverse *y* axis) during the last decade (2000–2010). Colored bars are from RG06, and white bars are from the highest rain gauge (RG31; elevation 1363 m) in the study site. (c) A scatterplot of monthly precipitation between two rain gauges (RG06 and RG31) from 2000. All units are mm.

relationship with the fraction of absorbed photosynthetically active radiation (FPAR) across different biome types [*Sellers*, 1985; *Asrar et al.*, 1992; *Myneni and Williams*, 1994; *Myneni et al.*, 2002], an indicator of energy absorption by vegetation and subsequent carbon uptake based on light use efficiency. Third, the nonlinear relationship between NDVI and LAI is highly site-specific depending on biome types and canopy structures [*Myneni et al.*, 2002], so it may introduce significant error during the transformation without field observations.

Table 1. Topographic Characteristics and Hydrologic Vegetation Gradients (HVG) of Headwater Catchments[a]

ID	Area (ha)	Elevation (m)	Slope (deg)	Transformed Aspect	Mean of TI	Skewness of TI	Mean DFL (m)	Average NDVI	HVG (*d*NDVI/*d*TI)	Disturbance History[b]
WS01	15.5	832	27.1	0.587	4.39	1.68	78.1	0.041	0.0000	white pine planted in 1957
WS02[c]	13.1	856	27.2	0.752	4.50	1.54	129.0	0.484	−0.0017	control
WS06	8.7	792	26.1	−0.315	4.17	1.83	52.2	0.407	0.0022	
WS07[c]	58.9	902	28.6	0.516	4.35	1.55	125.6	0.517	−0.0023	clear-cut in 1977
WS10	89.5	972	26.2	0.317	4.35	1.70	113.9	0.506	0.0033	
WS13	16.3	821	26.0	−0.051	4.20	2.12	90.0	0.518	−0.0111	
WS14[c]	62.4	878	25.7	−0.358	4.42	1.93	90.9	0.476	−0.0024	control
WS17[c]	13.6	895	28.7	−0.624	4.42	1.17	114.3	0.058	−0.0069	white pine planted in 1956
WS18[c]	12.3	823	28.1	−0.473	4.33	1.72	141.3	0.445	0.0131	control
WS19	28.3	957	24.8	−0.479	4.46	1.64	121.4	0.490	−0.0010	
WS21	24.6	989	24.0	−0.740	4.66	1.35	244.2	0.506	0.0012	control
WS22	35.7	1038	26.8	−0.646	4.46	1.64	153.2	0.522	−0.0006	
WS27[c]	39.8	1256	28.5	−0.636	4.67	1.48	146.4	0.489	0.0063	control
WS28	143.1	1212	25.7	−0.125	4.78	1.39	180.9	0.549	0.0141	
WS31	34.2	970	23.8	−0.211	4.52	1.74	115.4	0.492	0.0110	
WS32	40.6	1049	24.1	0.089	4.38	2.00	117.6	0.554	0.0049	control
WS34	32.6	1019	27.4	0.438	4.35	1.79	99.6	0.482	0.0083	control
WS36[c]	48.7	1289	30.5	0.345	4.68	1.30	189.3	0.451	0.0250	control
WS37[c]	44.1	1313	35.0	−0.259	4.62	1.24	186.1	0.497	0.0224	clear-cut in 1963, no removal
WS40	20.5	1055	31.5	0.609	4.15	1.94	126.2	0.546	0.0009	control

[a]TI, topographic wetness index; DFL, downslope flow path length; NDVI, normalized difference vegetation index.
[b]Details of disturbance history are available at http://coweeta.uga.edu/sitehistory.
[c]Gauged watersheds.

[14] Skewness of the TI distribution is also calculated as a topographic description of the headwater catchments [*Ducharne et al.*, 2000]. We hypothesize that more positive skewness is related to shorter flow path length to streams within the catchment. Mean downslope flow path length (DFL) to streams is also calculated for all headwater catchments to confirm this hypothesis using Terrain Analysis System (TAS) GIS software [*Lindsay*, 2005].

2.3. Hydrologic Metrics

[15] Daily streamflow data at eight gauged catchments (Figure 1 and Table 1) from 1985 to 1995 are used to characterize the hydrologic regimes of headwater catchments. Five are control watersheds (unmanaged since 1927), WS07/37 were clear-cut, and WS17 was converted to eastern white pine (*Pinus strobus* L.; Table 1). At each catchment, the runoff ratio (RR; R/P), evapotranspiration (ET; $P - R$) estimates, and Horton index (HI) values are calculated using observed precipitation (P) and streamflow (R) during ten water years (1986–1995). HI represents the ratio of actual evapotranspiration (ET) to catchment wetting (W) following *Troch et al.* [2009]:

$$HI = \frac{ET}{W} = \frac{P - R}{P - S} \tag{2}$$

where S is storm runoff, calculated by a hydrograph separation from streamflow data. Catchment wetting (W) is the precipitation retained in the soil and available to vegetation. It is calculated by removing quick flow component. The Web-based Hydrograph Analysis Tool (WHAT) system [*Lim et al.*, 2005] is used to separate base flow from daily streamflow using the two-parameter digital filtering method [*Eckhardt*, 2005]. These simple metrics are calculated both on water year and seasonal basis (summer, JJA, and winter, DJF). Note that ET estimates implicitly include storage changes especially at seasonal time scales. This information expresses a dynamic response of each headwater catchment including its memory effect. Dominant deciduous broadleaf trees have fully extended and no leaves during summer and winter seasons, respectively [*Hwang et al.*, 2011].

2.4. Recession Slope Analysis

[16] *Brutsaert and Nieber* [1977] proposed a well-known recession analysis by plotting the observed recession slope ($-dQ/dt$) with the discharge (Q) using a power function of the form

$$\frac{dQ}{dt} = -aQ^b \tag{3}$$

The recession slope analysis has been widely used to investigate groundwater aquifer characteristics, such as soil and geomorphic parameters using analytical solutions to the one-dimensional Boussinesq equation. Even though the parameterization of the analytical solution was originally developed for unconfined horizontal aquifers in homogeneous soils, several analytical solutions have been also developed for sloping aquifers in heterogeneous soils [see *Rupp and Selker*, 2006b].

[17] In these solutions, the parameter a is usually related to hydraulic properties of groundwater aquifers, while the exponent b is set to be constant. The exponent b however has been shown to vary between different watershed and within a given watershed under different flow conditions [*Tague and Grant*, 2004; *Szilagyi et al.*, 2007]. The exponent b reflects the degree of nonlinearity of the storage-discharge relationship. Within a watershed, the storage-discharge relationship (b) may change with current moisture conditions, reflecting changes in the spatial extent of watershed connectivity or shifts in the distribution of drainage characteristics associated with currently active aquifers. Differences in recession slope among hillslopes or watersheds reflect differences in drainage properties, their heterogeneity, and spatial organization [*Rupp and Selker*, 2006b; *Tague and Grant*, 2004; *Harman et al.*, 2009]. In this paper, we use recession slope analysis to identify transitions in dominant flow regimes over the time distribution of flows within and across different headwater catchments.

[18] Recession slope analysis is applied to long-term daily streamflow records (1985–1995) at eight gauged headwater catchment during the recession period, defined as any day of decreasing flow without precipitation. We use the "scaled-dt" recession slope analysis, which allows time interval (dt) to be adjusted to $-dQ$ values rather than to be constant [*Rupp and Selker*, 2006a]. The recession coefficients are computed using reduced major axis regression (organic correlation) as both $-dQ/dt$ and Q values are subject to error [*Brutsaert and Lopez*, 1998; *Hirsch and Gilroy*, 1984].

[19] We also apply several thresholds in $-dQ/dt$ values (0.01, 0.1, 0.2, and 0.3 mm d^{-2}) in the analysis to remove small $-dQ/dt$ values for several reasons. First, these small values are more affected by other concurrent hydrological processes (e.g., channel hydraulics) that alter apparent recession behavior. Second, small $-dQ/dt$ values are sensitive to uncertainty and error in observations, including detection limits and rating curve calibration. Third, small $-dQ/dt$ values that usually happen during late recessions possibly better represent hydraulic characteristics of deep groundwater aquifers, decoupled with shallow-rooted vegetation water use in the study site. Note that *Brutsaert and Nieber* [1977] originally used lower envelopes of scatter plots to estimate deep groundwater aquifer characteristics assuming the minimum recession rate ($-dQ/dt$) at a given Q would solely depend on deep groundwater storage. The resulting slope b and intercept $\log(a)$ coefficients at different thresholds are then plotted against the HVG values.

2.5. Semidistributed Ecohydrological Model (RHESSys)

[20] Regional Hydro-Ecological Simulation System (RHESSys) is a GIS-based, ecohydrological modeling framework designed to simulate carbon, water, and nutrient cycling in complex terrain [*Band et al.*, 1993; *Tague and Band*, 2004]. RHESSys combines a set of physically based process models and a methodology for partitioning and parameterizing the landscape. The spatially distributed structure enables the modeling of spatiotemporal interactions between different ecohydrological processes from patch to watershed scales. RHESSys has two options for lateral redistribution of water within a catchment: one derived from the routing approach in the distributed hydrology soil vegetation model (DHSVM) [*Wigmosta et al.*, 1994] and a quasi-distributed approach to hillslope hydrological processes based on TOPMODEL

[*Beven and Kirkby*, 1979]. In this study, the TOPMODEL approach is used.

[21] The model simulates the subsurface flow ($Q_{subsurface}$) under the assumption of the exponential decay of saturated hydraulic conductivity with soil depth.

$$Q_{subsurface} = T_0 \cdot e^{-\lambda} \cdot e^{-s/m} \quad (4)$$

where T_0 is the effective lateral saturated transmissivity (m^2 d^{-1}), λ and s are the mean TI and water equivalent water table depths (m) within the hillslope, and m is the decay rate of hydraulic conductivity with depth (m).

[22] RHESSys is applied to the eight gauged headwater catchments (Table 2 and Figure 1) with a 10 × 10 m grid resolution during three water years (1991–1993) with a 9 month spin-up period. The spatial pattern of maximum leaf area index (LAI) is prescribed in the model without interannual variation, estimated by regressing NDVI and various LAI observations [*Hwang et al.*, 2009]. The seasonal pattern of LAI in coniferous watersheds (WS01/17; Figure 1) is also prescribed from previous field observations without spatial variations [*Vose and Swank*, 1990; *Vose et al.*, 1994]. A normalized vegetation phenology from 10 year Moderate-resolution Imaging Spectroradiometer (MODIS) NDVI (2000–2009) for each headwater catchment [*Hwang et al.*, 2011] is also prescribed in the model. Other ecophysiologic and soil parameterizations are based on detailed field observations within the study site [*Hwang et al.*, 2009; *Hales et al.*, 2009].

[23] Three daily climate inputs (max and min temperature and precipitation) are used in the model. The closest climate station and rain gauge from each headwater catchment are used as a base station in the model (Figure 1), from which spatial daily inputs of temperature and precipitation are extrapolated on the basis of temperature lapse rates [*Bolstad et al.*, 1998b] and a long-term isohyet map. The long-term isohyet is developed using universal cokriging with 5 year total precipitation (1991–1995) from nine rain gauges within the study site (Figure 1).

2.6. Generalized Likelihood Uncertainty Estimation

[24] Generalized Likelihood Uncertainty Estimation (GLUE) methodology is used to estimate behavioral parameter ranges in each headwater catchment rather than choosing a single optimum [*Beven and Binley*, 1992; *Freer et al.*, 1996]. GLUE associates different degrees of belief to behavioral parameter sets by weighting with likelihood values, where it is accepted as behavioral if a model run satisfies certain criteria. The behavioral parameter sets are then ranked to form a cumulative probability distribution to produce uncertainty bounds from selected quantiles. The Nash-Sutcliffe efficiency [*Nash and Sutcliffe*, 1970] for the log of daily streamflow is used as a likelihood measure in this study, as it emphasizes low flows (rather than peaks) that are coupled with vegetation water use [e.g., *Bond et al.*, 2002].

[25] The model is calibrated with three TOPMODEL parameters, the decay rate of hydraulic conductivity with depth (m), the effective lateral saturated transmissivity ($\ln(T_0)$), and the vertical saturated hydraulic conductivity ($K_{sat0.vert}$). Monte Carlo simulation is implemented four thousand times from uniform distributions within prescribed ranges. Simulation sets above the 97.5% upper quantiles ($n = 100$) are set as behavioral to effectively constrain parameter ranges in different headwater catchments. Likelihood measures and behavioral parameter ranges are also calculated on a seasonal basis using the behavioral thresholds (Table 2). The seasonal behavioral parameter ranges help us to understand the model dynamics and the seasonal variation of hydrologic responses under the TOPMODEL framework [*Freer et al.*, 2004].

2.7. Statistical Analysis

[26] A multiple regression analysis is used to relate HVG to topographic variables including area, elevation, slope, transformed aspect, and skewness of the TI distribution for all headwater catchments ($n = 20$; Table 1). All interaction terms of the topographic variables are included in the analysis. To minimize the risk of overparameterization, the automatic model simplification function *stepAIC* in package MASS version 7.2 for R (The R Foundation for Statistical Computing) is used for parsimonious models, which performs stepwise model selection by a penalized log likelihood method (Akaike's information criterion).

3. Results

3.1. HVG and Topographic Characteristics

[27] Two high-elevation catchments (WS36/37) have relatively high HVG values (Figure 3 and Table 1), while two low-elevation south facing (WS02/07) and the coniferous (WS17) catchments are negative. The two north facing hardwood catchments (WS18/27) have medium HVG values. Two low-elevation control catchments (WS02/18) have HVG of opposite sign even though their topographic characteristics are very similar except for aspect (Table 1).

Table 2. Maximum and Threshold Nash-Sutcliffe Efficiency Values

	Full Year		Summer Season (June–August)		Winter Season (December–February)	
ID	Maximum	Threshold	Maximum	Threshold	Maximum	Threshold
WS02	0.866	0.842	0.867	0.810	0.800	0.770
WS07	0.886	0.855	0.755	0.679	0.904	0.856
WS14	0.878	0.844	0.805	0.729	0.854	0.809
WS17	0.869	0.845	0.849	0.771	0.823	0.795
WS18	0.894	0.867	0.841	0.769	0.869	0.843
WS27	0.896	0.858	0.857	0.804	0.937	0.887
WS36	0.831	0.789	0.745	0.703	0.849	0.812
WS37	0.809	0.755	0.772	0.695	0.835	0.747

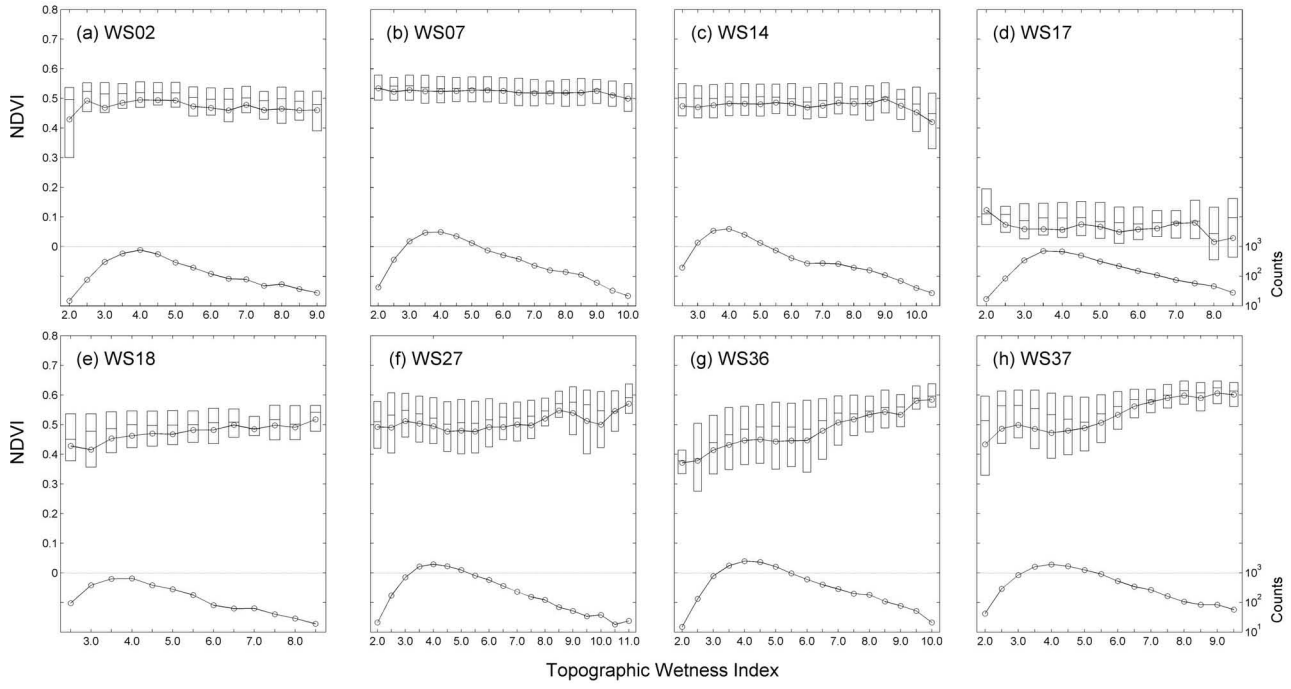

Figure 3. Vegetation patterns along the hydrologic flow paths at eight gauged headwater catchments. Circles represent average NDVI values, and box plots denote the lower quartile, median, and upper quartile values for each binned group. Counts are numbers of 6.1 m patches. Hydrologic vegetation gradients (HVG) are simply calculated from a linear regression of average NDVI values.

Two coniferous catchments (WS01/17) are featured with relatively low NDVI values and vegetation gradients, paired with adjacent control catchments (WS02/18). Catchments have very diverse combinations of elevation, aspect, and skewness values (Table 1). WS14 has the highest skewness of the TI distribution with the highest order of streams among the gauged catchments, whereas WS17 has the lowest. WS36 and WS37 also have relatively low skewness values. These skewness values show significant negative correlation to the mean DFL to streams (Figure 4; $R^2 = 0.475$, $P < 0.001$) for all headwater catchments ($n = 20$). This indicates that the catchments with larger TI distribution skewness have larger drainage density and shorter flow path length to the streams in the study area.

3.2. HVG and Hydrologic Metrics

[28] The relationships between the observed HVG and hydrologic metrics are shown in Figure 5. The RR (runoff ratio), ET (evapotranspiration), and HI (Horton index) values have significant linear relationships with HVG. All low-elevation catchments maintain similar levels of RR, ET, and HI values even during the winter when soil recharge is active. This indicates that vegetation at low-elevation catchments likely experiences more water stress than high-elevation catchments during the summer. However, three high-elevation catchments (WS27/36/37) show dramatic differences in seasonal RR, ET, and HI values, which suggests weaker memory effect of the system than low-elevation catchments. Vegetation gradients have more significant relationships with annual hydrologic metrics, which better represent the system-wide long-term hydrologic connectivity. These relationships are least significant during the summer season, when RR, ET and HI values of deciduous broadleaf catchments are much more similar.

[29] The coniferous catchment (WS17) has the lowest RR, the highest ET and HI values of all catchments, while

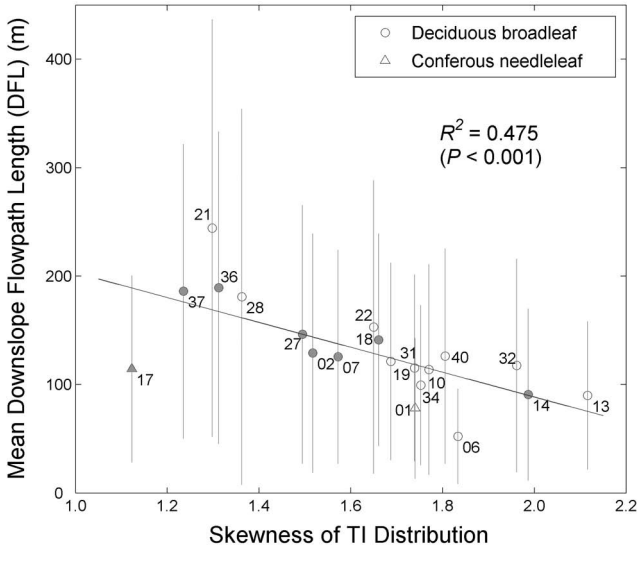

Figure 4. Relation between the skewness of the topographic wetness index (TI) distribution and the mean downslope flow path length (DFL) to streams (m) for all headwater catchments (Table 1 and Figure 1). Vertical lines represent the standard deviations of DFL within the catchments. The gauged catchments are shaded gray.

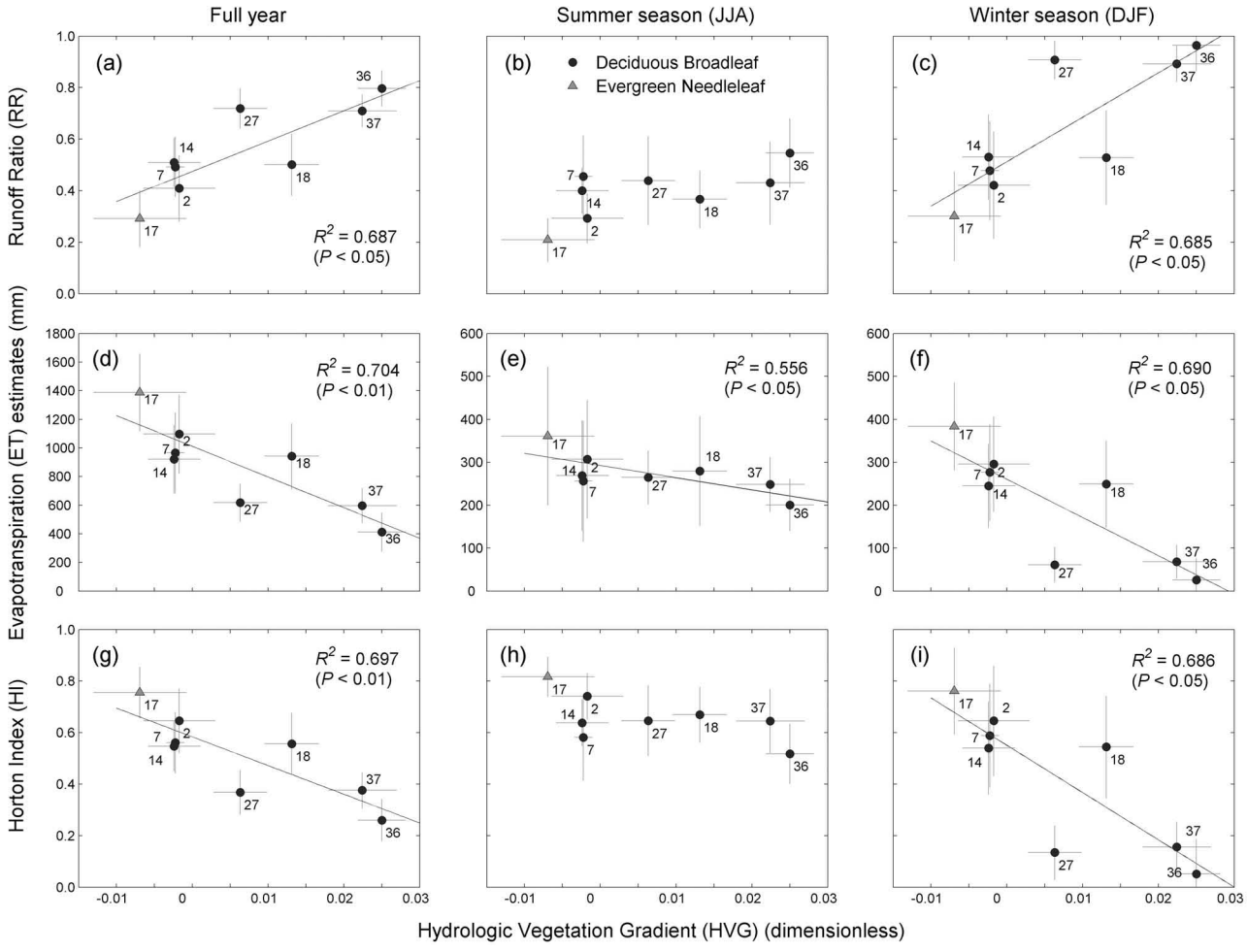

Figure 5. Relation between HVG and hydrologic metrics during (left) the full year, (middle) the summer (June–August), and (right) the winter season (December–February) for eight gauged headwater catchments. Vertical and horizontal bars represent standard deviations during a 10 water year period (1986–1995) and 95% confidence intervals of estimated HVG, respectively.

the south facing low-elevation catchment (WS02) has the highest ET and HI values among the deciduous broadleaf catchments. Three high-elevation catchments (WS27/36/37) show relatively high RR, low ET and HI values compared to low-elevation catchments, as well as larger seasonal differences. In high-elevation catchments, interannual variations of RR during the summer season are higher than those from low-elevation catchments, while estimated ET and HI interannual variations are lower. This indicates that vegetation water use at high elevation is consistently maintained within certain ranges regardless of precipitation variation as water stress rarely experienced due to high precipitation and low temperature (Figure 2c). However, interannual variations of ET in low-elevation catchments are higher than those at high elevation, which represents the greater dependency of vegetation water use on the interannual hydroclimate variability. HI values during the full year and summer season have lower interannual variation compared to RR and ET (Figure 5). This may indicate that the HI efficiently excludes the interannual effect of climatic variables and better represents vegetation condition than RR and ET values [*Troch et al.*, 2009].

3.3. HVG and Recession Behavior

[30] The recession slope analyses for eight gauged headwater catchments are shown in Figure 6. Higher R^2 values and narrower scatter ranges are observed in high-elevation catchments (WS27/36/37), which indicate more uniform hydrologic responses at a given Q. A more uniform recession slope across flow conditions for the high-elevation catchments is consistent with more uniform degree of within hillslope connection. In other words, because these catchments maintain greater levels of moisture (closer to saturation) throughout the year, the dominant aquifer (and its properties) for a given Q does not change substantially. For low-elevation catchments, the exponent b gradually decreases with larger $-dQ/dt$ thresholds while the intercept $\log(a)$ increases. This suggests that the shape of recession curves in these catchments fluctuates more than those from the high-elevation catchments across antecedent recharge history primarily because of higher evaporative demand and lower precipitation (Figure 2). In other words, the short-term responses of these catchments (also called "impulse responses") are relatively decoupled with their long-term

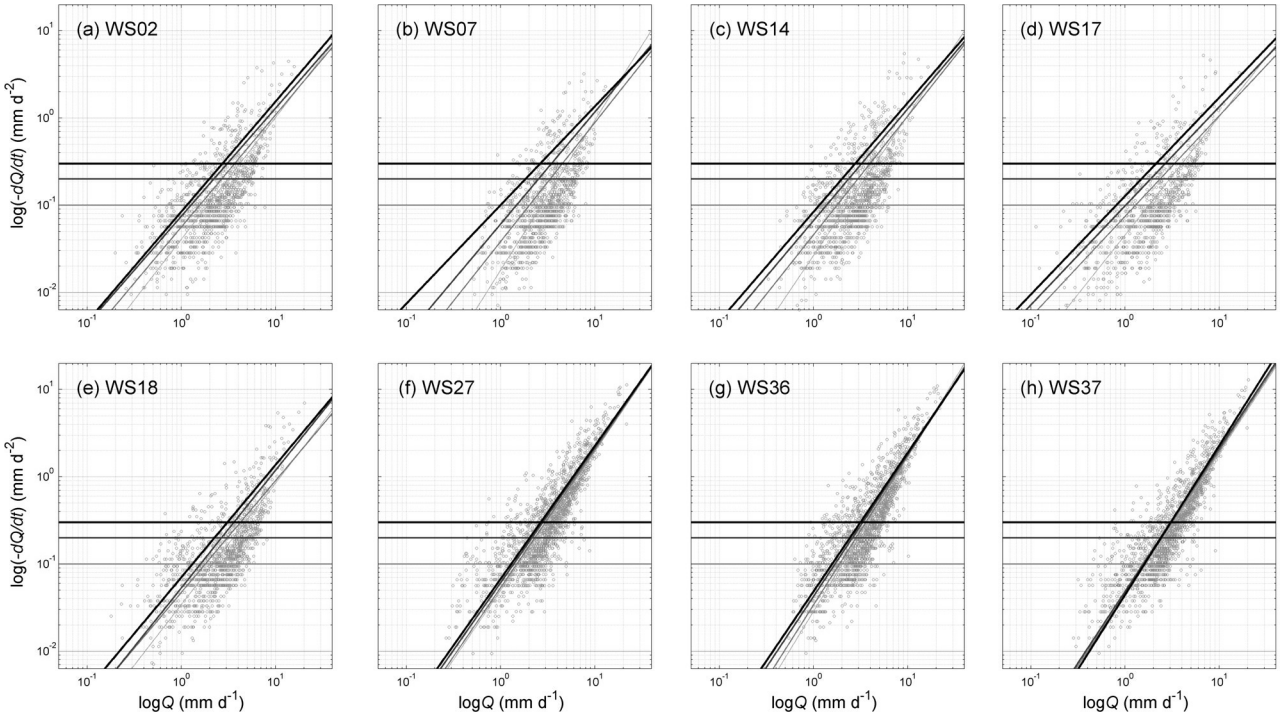

Figure 6. Recession slope analyses (log Q versus log($-dQ/dt$)) for eight gauged headwater catchments. Regression lines are calculated with different thresholds (0.01, 0.1, 0.2, and 0.3 mm d^{-2}), where each regression line corresponds to the horizontal threshold line with the same color and thickness. All regression lines are statistically significant ($P < 0.001$).

responses, featured by the upper and lower envelopes in the recession slope analysis, respectively (Figure 6).

[31] Further comparisons between recession coefficients and HVG values are given in Figure 7. HVG values show strong negative linear relationships with the intercept log(a) only at 0.20 and 0.30 threshold levels. This indicates that early recessions with high $-dQ/dt$ values are closely linked to HVG-derived hydrologic connectivity, while late recessions with low $-dQ/dt$ values rather represent the characteristics of deeper groundwater aquifers. A higher intercept reflects a more rapid recession and thus more efficient drainage system for a given Q, where upslope drainage is less available to vegetation downslope (smaller HVG).

[32] The exponent b values are largely scattered at two ranges: around 1.5 for high-elevation catchments and 1.0 for low-elevation catchments. This suggests that the drier low-elevation catchments behave more like a linear storage system, while wetter high-elevation catchments show strong nonlinear behavior. *Brutsaert and Nieber* [1977] demonstrated that the nonlinear Boussinesq solution produces a slope of 1.5 for long-time solutions, very close to those from high-elevation catchments reported here. *Rupp and Selker* [2006b] also showed that the exponent b in sloping aquifers would be expressed with vertical heterogeneity of saturated hydraulic conductivity, ranged from 1 to 2. This also reflects the transitions in dominant flow regimes from deeper groundwater flow to shallow subsurface flow along the elevation gradient due to associated environmental temperature lapse rate coupled with strong orographic precipitation patterns (Figure 2c).

3.4. HVG and Behavioral TOPMODEL Parameters

[33] Maximum likelihood measures and threshold values for behavioral parameter sets (Table 2) show that the model efficiently captures the different runoff regimes of each headwater catchment. The model usually performs better during the winter season than the summer season. Simulated uncertainty bounds of daily streamflow from behavioral parameter sets are shown in Figure 8. The model effectively simulates different levels of low flows during the growing season. However, the model significantly underestimates peak flows for two high-elevation catchments (WS36/37) especially during high-flow periods. This may occur because of inaccuracy of precipitation inputs as there are no close rain gauges for these two catchments (Table 2 and Figure 1), and calibration uses the log of streamflow which would better capture low-flow behavior.

[34] The relationships between HVG and behavioral parameter ranges during the full year and summer season are shown in Figure 9. During the summer season, the m and ln(T_0) parameters show correlations with the vegetation gradients, as well as a negative covariance between them. With an HVG increase, behavioral m ranges largely increase while behavioral ln(T_0) ranges decrease. The TOPMODEL framework accounts for the hydrologic connectivity between upslope and downslope regions with the key m parameter, controlling the range of a local water table depth from their mean on the basis of the TI distribution [*Beven and Kirkby*, 1979]. It indicates that larger m values in TOPMODEL not only represent higher vertical heterogeneity of soils by definition, but also more upslope subsidy of water along

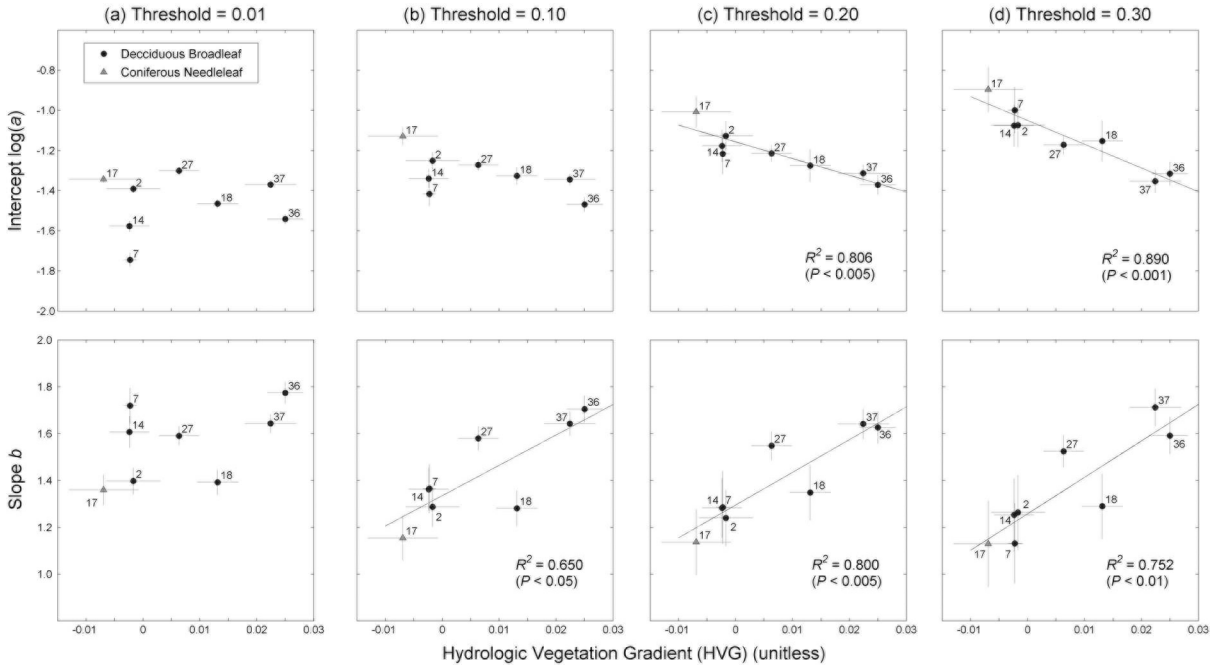

Figure 7. The relationships of hydrologic vegetation gradients (HVG) with (top) the intercept log(a) and (bottom) the slope b values from the regression slope analysis with different threshold values: (a) 0.01, (b) 0.1, (c) 0.2, and (d) 0.3 mm d^{-2}.

hydrologic flow paths, The parameter m is also related to the slope of the recession curves (equation (4)), where a higher m reflects less steep hydrograph recessions [*Freer et al.*, 2004]. This also means that the steeper recessions during the summer season represent a more disconnected hillslope within the catchment, and less chance for upslope subsidy to be used by vegetation downslope. It is worthwhile to note that two possible outliers in Figure 9b are represented by catchments with the highest skewness of TI distribution (WS14) and the most recent disturbance history (a commercial clear-cut in 1977; WS07; Table 1). With these outliers removed, there is a more significant relation between HVG and behavioral m ranges with an exponential model ($R^2 = 0.89$; $P < 0.01$).

[35] HVG show less significant relationships with the behavioral parameter ranges of the other seasons. This suggests that HVG is more related to the pattern of low flows, and effectively represents the level of water subsidy along hydrologic flow paths during the growing season. Instead, the behavioral m ranges of deciduous headwater catchments during the winter season are significantly related to the skewness of TI distribution and the mean DFL to streams (Figure 10). Interestingly, the coniferous evergreen catchment (WS17) occupies distinct parameter spaces in Figure 10, where vegetation water use is still active even during the winter. The seasonal fluctuations of behavioral m parameter also reflect a structural deficiency of TOPMODEL from the steady state assumption related to overestimation of upslope contributing area especially during dry periods (the so-called dynamic a problem) [*Beven and Freer*, 2001]. In addition, high-elevation catchments also show very distinct RR, ET and HI values during the winter season (Figures 5c, 5f, and 5i). These surely indicate that the flow levels during the winter season are more related to catchment topology and topoclimatic factors rather than vegetation water use.

3.5. Topographic Controls on HVG

[36] Two multiple regression models for HVG with topographic variables are summarized in Table 3. The model shows a higher R^2 value without two coniferous catchments (WS01/17), which have very different phenological patterns and resulting seasonal patterns of evapotranspiration. Elevation shows significant positive relationships with vegetation gradients in both models. This suggests that there is more lateral hydrologic connectivity at higher elevation, reflecting the combined effect of orographic precipitation and environmental temperature lapse rate along the elevation gradient (Figure 2).

[37] The significance of the interaction term between transformed aspect and slope can be interpreted as strong radiative controls on hydrologic connectivity as this multiplicative term is a typical radiation proxy parameter in steep terrain [*Pierce et al.*, 2005]. More vegetation water use on south facing slopes results in less hydrologic connectivity during the growing season and smaller HVG within the catchment. This result is also consistent with the comparison between two low-elevation control watersheds at different slopes (WS02/18).

[38] The skewness of TI distribution shows a significant negative relationship with vegetation gradients for deciduous catchments (Table 3). Considering that the skewness has a significant negative relationship with the mean DFL to streams (Figure 4), it indicates that upslope subsidy may not be used efficiently by downslope vegetation in hillslopes with short DFL. Note that WS14, which has the

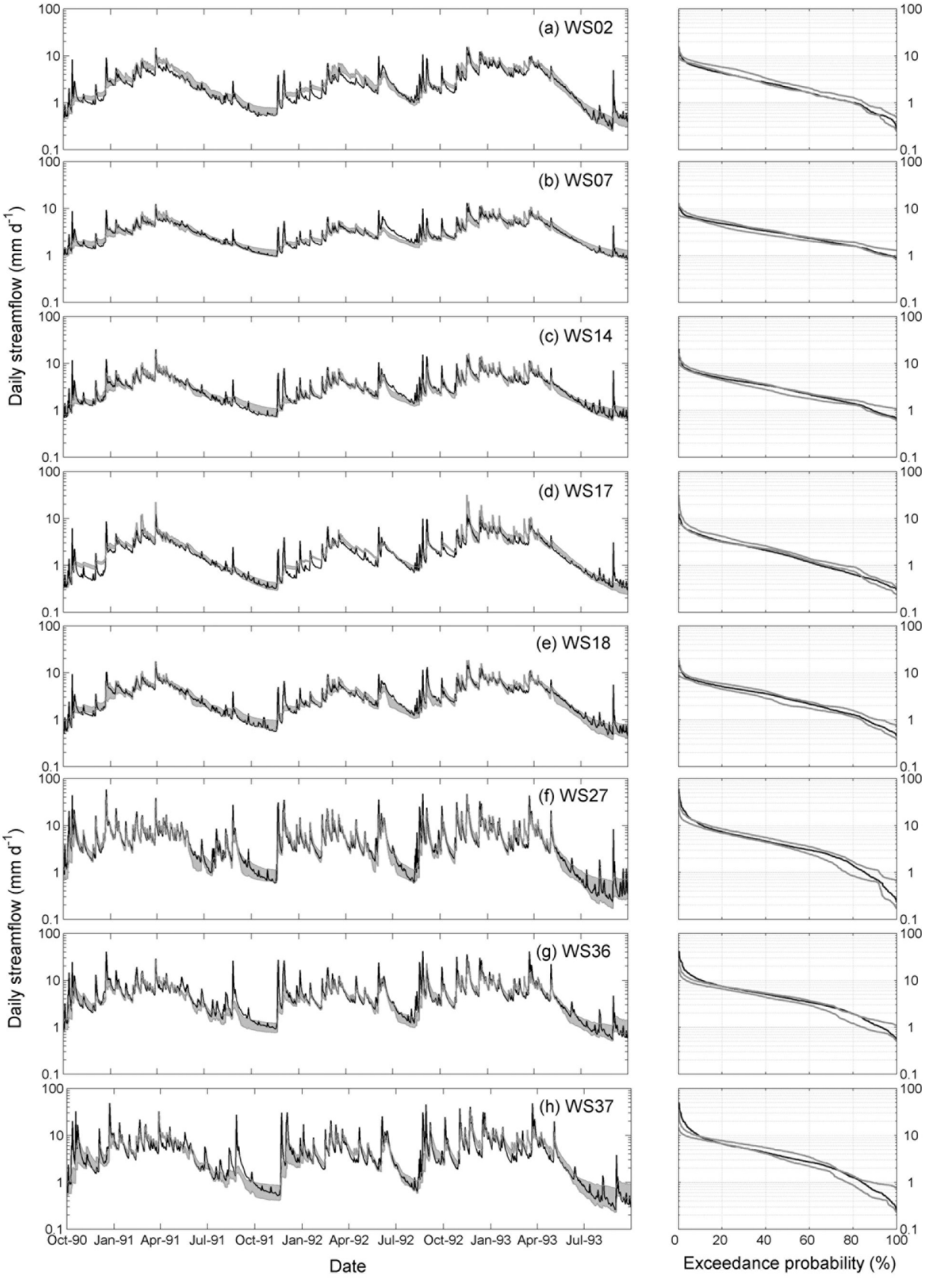

Figure 8. Observed daily streamflow (black) and 5%/95% uncertainty boundaries (gray) from behavioral parameter ranges (Table 2) and their exceedance probabilities (%) for eight gauged headwater catchments during 3 water year simulations (1991–1993; Table 2).

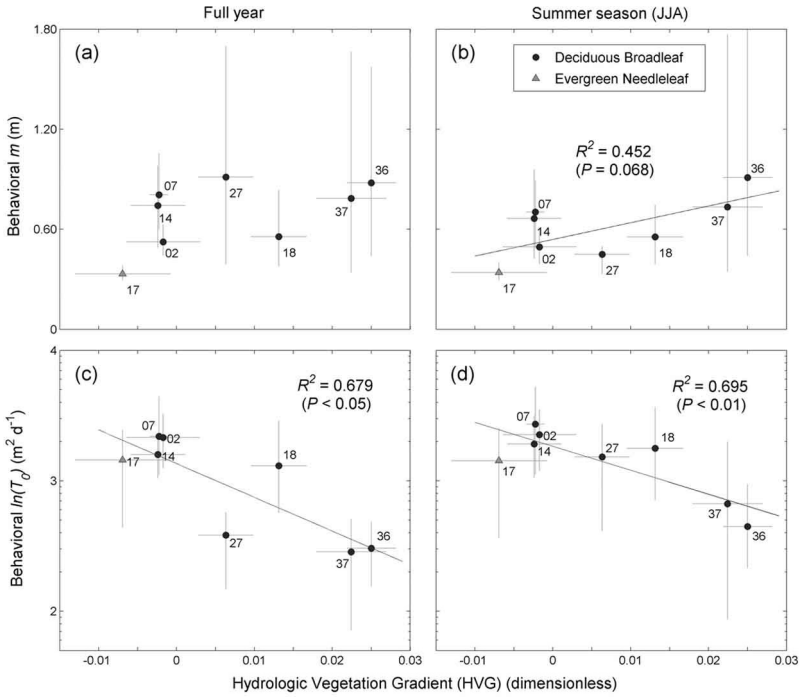

Figure 9. Relation between HVG and the behavioral ranges of two key TOPMODEL parameters (m and $\ln(T_0)$) during the full year (left column) and the summer season (JJA; right column).

highest skewness and the lowest DFL values among gauged catchments (Figure 4), occupies a unique position during the summer season (Figure 9b). This can be interpreted as a dominant geomorphic control on long-term hydrologic connectivity especially during the dormant season. The catchment area variable does not show any significance to vegetation gradients. This is consistent with previous studies, which reported no significant effect of area on hydrologic connectivity [*McGlynn et al.*, 2004].

4. Discussion

[39] In this study, HVG in headwater catchments are estimated from fine resolution satellite imagery, and are related to hydrologic metrics, recession coefficients, and behavioral parameter ranges for a quasi-distributed ecohydrological model. Vegetation gradients are significantly correlated to annual hydrologic metrics (RR, ET, and HI). In addition, vegetation gradients are also related to early recession behavior represented by recession coefficients and behavioral parameter ranges of TOPMODEL. Increased vegetation density along hydrologic flow paths suggests substantial water subsidy from upslope to downslope especially through shallow subsurface flow that is the main source of streamflow in this region [*Hewlett and Hibbert*, 1967]. On the contrary, static or decreased vegetation density downslope indicates more localized water use by vegetation and less lateral hydrologic connectivity especially during the growing season. Specifically, negative HVG indicates that downslope vegetation may experience more water stress because of associated temperature increases and orographic precipitation decreases at low elevations. The decrease of NDVI downslope may also be related to low-NDVI species (e.g., rhododendron, eastern hemlock) in cove region in the study area [*Day et al.*, 1988; *Bolstad et al.*, 1998a].

[40] The exponent b effectively represents the dominant flow regimes of upslope subsidy. The upslope subsidy in catchments with large HVG is dominated by shallow subsurface flow, represented by large exponent b (around 1.5). The catchments with small HVG are probably more dominated by deeper groundwater flows as they behave like a simple linear storage system featured by small b (around 1.0). Therefore, streams are disconnected from upslope, and hydrologic responses are spatially limited to the near-stream (riparian) dynamics in these catchments. There are fewer chances for upslope subsidy to be taken by vegetation downslope, as the rooting depths in this region are quite shallow (around 1 m) and rather spatially uniform [*Hales et al.*, 2009]. The early recession behavior is also closely related to HVG. Smaller HVG headwater catchments usually have steeper early recessions, featured by large intercept, $\log(a)$ denoting more efficient drainage, and small behavioral m parameter ranges. Note that the recession behavior is not only associated with dominant flow regimes, but also with drainage efficiency of headwater catchments.

[41] We also found that the skewness of TI distribution has a significant positive relationship with behavioral m parameter ranges during the winter season (Figure 10a) and a statistically significant negative relationship with HVG for deciduous catchments (Table 3). Considering that skewness is a major factor determining the saturated fraction in TOPMODEL [*Ducharne et al.*, 2000] as well as its relationship with mean DFL to streams (Figure 4), it may be interpreted as a significant geomorphic control on hydrologic response. This is closely related to drainage efficiency

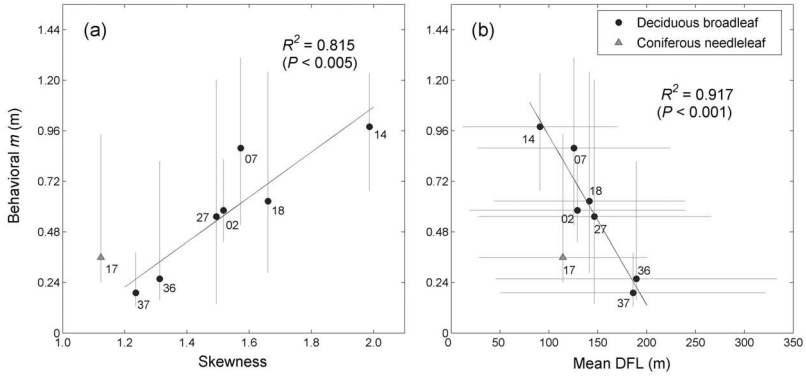

Figure 10. Relation between (a) the skewness of the TI distribution and (b) the mean downslope flow path length (DFL) to streams with the behavioral *m* parameter ranges during the winter season (December–February). Vertical lines represent 5% and 95% uncertainty boundaries. Horizontal lines represent the standard deviations of DFL to streams within the catchments. The evergreen coniferous catchment (WS17) is excluded for the linear regression analyses.

(or density) and channel network structure within the catchment [*Woods and Sivapalan*, 1997]. *Thompson et al.* [2011] found the self organization of vegetation cover driven by lateral subsidies is primarily determined by climate, drainage density, and vegetation water use using a simple network water balance model for both vegetation distribution and catchment water balance. *Voepel et al.* [2011] also demonstrated that Horton index values are significantly related to topographic characteristics (elevation, slope) in addition to climatic factors.

[42] Vegetation has priority for precipitation and soil water through interception and transpiration [*Brooks et al.*, 2010]. Therefore, vegetation patterns within headwater catchments effectively represent the pattern of soil water partitioning between localized water use by vegetation (so-called green water) and lateral hydrologic flows (so-called blue water). In this sense, green water downslope is partially dependent on the generation of blue water upslope. The interactive role of vegetation with hydrologic connectivity is first confirmed by the comparison of two first-order control catchments with opposite aspects (WS02/18; Table 1). In spite of the similarity in topographic characteristics and the amount of total precipitation, they have very different RR, ET, and HI values (Figure 5), recession coefficients (Figure 7), and behavioral parameter spaces (Figure 9). We also found that the multiplicative term of transformed aspect and slope has a significant negative relation with vegetation gradients (Table 3). Greater radiation loads on steep south facing slopes and resulting increased evapotranspiration demand cause more localized water use than on north facing slopes, which decreases lateral hydrologic connectivity and spatial organization of vegetation along the hydrologic flow paths.

Table 3. Summary of Two Multiple Regression Models for the Hydrologic Vegetation Gradient of Headwater Catchments[a]

	Model 1 ($n = 20$)	Model 2[b] ($n = 18$)
elevation	4.48×10^{-5} ****	2.87×10^{-5} **
elevation : taspect[c]	5.22×10^{-5} *	9.27×10^{-5} ****
taspect : slope[c]	-1.79×10^{-3} *	-3.33×10^{-3} ****
skewness[d]		-1.85×10^{-2} **
R^2	0.637	0.877

[a]Asterisks indicate the following: ****, $P < 0.0001$; ***, $P < 0.001$; **, $P < 0.01$; *, $P < 0.05$.
[b]Two coniferous watersheds (WS01/17) are excluded.
[c]*taspect*, transformed aspect.
[d]Skewness of the TI distribution.

[43] The importance of radiative controls on hydrological processes has been investigated by a number of hydrologic and ecosystem studies. *Broxton et al.* [2009] reported primary controls of aspect on transit times in semiarid and snow-dominated environments with shorter transit times in south facing slopes with less vegetation cover. *Ivanov et al.* [2008] pointed out that the aspect and slope are the key factors determining distributed hydrologic behavior and resulting vegetation patterns in a semiarid region. Many studies found that aspect was an important factor in soil water redistribution [e.g., *Moore et al.*, 1988; *Western et al.*, 1999]. A number of sap flux studies also found that heterogeneity of available light is a significant factor explaining the spatial variation in transpiration [*Ewers et al.*, 2007; *Burgess and Dawson*, 2008; *Loranty et al.*, 2010]. The spatial variability of incoming solar energy at different topographic positions results in different ecohydrological patterns of vegetation, evapotranspiration, timing/intensity of snowmelt, resulting streamflow generation, and even geologic-scale soil development [e.g., *Hwang et al.*, 2011; *Istanbulluoglu et al.*, 2008].

[44] Larger HVG in high-elevation catchments (WS36/37; Table 1) and the strong significance of elevation to HVG (Table 3) are associated with topoclimatic controls on lateral hydrologic connectivity; strong orographic precipitation patterns [*Swift et al.*, 1988] and the environmental temperature lapse rate [*Bolstad et al.*, 1998b] in the study area. Lower potential evapotranspiration and higher precipitation at high elevations (Figure 2) result in more dominance of lateral hydrologic flows, which leads to high RR, low HI, larger recession coefficient *b*, and higher HVG (Table 1 and Figure 5).

[45] In this study, we have found that the HVG typically decreases with increasing HI. This relationship may not be applicable in ecosystems that are not water limited. In energy-limited ecosystems, HVG may be largely determined by confounding elevational or radiation changes along hydrologic flow paths. A postulated relationship between HI and HVG is shown in Figure 11 when hypothetical mountainous

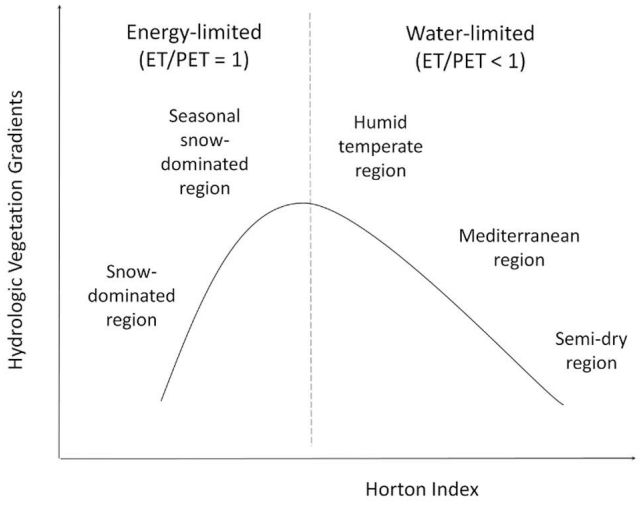

Figure 11. A postulated relationship between Horton index and HVG. ET, evapotranspiration; PET, potential evapotranspiration.

headwater catchments would be located in different climate regions. In a snow-dominated climate region, the catchment may have the lowest HI as well as low vegetation gradients. In seasonally snow-dominated ecosystems, vegetation appears downslope first where temperatures are usually higher. *Tague* [2009] also reported that the upslope subsidy through seasonal snowmelts possibly decreased plant water stress downslope in a mountainous watershed in the Sierra Nevada. In this case, the vegetation gradients increase with the increase of HI, opposite to what is suggested in this study (Figure 5). In more water-limited regions, the vegetation gradients would decrease when HI increases.

[46] The high-elevation region in Coweeta may be more energy limited than water limited because of low temperature and high precipitation. The region around the 1100–1300 m elevation band is usually regarded as the transition zone from southern Appalachian to northern hardwood forests [*Day et al.*, 1988]. Additionally, phenological features at high elevation are determined solely by temperature compared to low elevation [*Hwang et al.*, 2011]. In this sense, the larger HVG in high-elevation south facing catchments (WS36/37) may be mostly driven by the accompanying temperature gradient downslope as well as the geomorphic gradient of steep, landslide dominated areas with limited soil cover compared to deeper, organic soils downslope [*Band et al.*, 2012]. In addition, this may explain why we have a relatively low vegetation gradient in the high-elevation north facing catchment (WS27), with consistent energy limitations from ridge to valley. WS27 also lacks escarpments which drive the geomorphic gradients in soil depth and organic matter in WS36/37. It implies that HVG would be highest in the ecotone region (Figure 11), where limiting factors for vegetation growth vary along hydrologic flow paths.

[47] This study implicitly assumes that water (or accompanying nutrient) is a limiting resource for vegetation, and therefore vegetation patterns are mainly determined by the lateral redistribution of soil water driven by dominant flow regimes. However, even when vegetation patterns are determined by covarying factors along hydrologic flow paths (e.g., temperature, radiation, and soils), emergent vegetation itself can be used to estimate the level of long-term partitioning between localized water use and lateral water flow along hydrologic flow paths. In other words, the effect of covarying factors is already manifested in emergent vegetation patterns. Note that HVG suggested in this study is not intended for isolating the effect of soil moisture on vegetation density.

[48] Traditionally, in subhumid or humid mountainous catchments hydrologists have focused more on the topographic control of hydrologic processes [e.g., *McGuire et al.*, 2005; *Tetzlaff et al.*, 2009]. However, our study suggests that topography may exert primary controls over hydrologic response during high flows, while vegetation water use has a significant effect on hydrologic connectivity during the growing season. Therefore, the hydrologic response of watershed systems should be understood by competition between vegetation water use and drainage efficiency [*Thompson et al.*, 2011]. In this sense, this study suggests that emergent vegetation patterns within headwater catchments may be used as a diagnostic tool to understand the interaction of local water balance (vegetation water use or remnant soil recharge) along the hydrologic flow paths with lateral redistribution.

5. Conclusions

[49] In this study, we propose the hydrologic vegetation gradient (HVG) as a simple indicator for lateral hydrologic connectivity in a headwater catchment. HVG shows significant relationships with annual hydrologic metrics and the patterns of flow regimes during the growing season. Using HVG, we found dominant topoclimatic and geomorphologic controls on lateral hydrologic flows in the study area. Without significant disturbance, the spatial organization of vegetation within catchments effectively represents the degree of dependency of ecosystems along hydrologic flow paths. This study also presents the potential to estimate early recession behavior, and key model parameters of ungauged headwater catchments from remotely sensed HVG.

[50] **Acknowledgments.** We thank the Editor, Michael L. Roderick, and two anonymous reviewers for constructive comments. The research represented in this paper was supported by the National Science Foundation award to the Coweeta Long Term Ecologic Research project (DEB 0823293). The USDA Forest Service provides long-term streamflow and climate data, as well as access and facilities at the Coweeta Hydrologic Laboratory.

References

Ali, G. A., and A. G. Roy (2010), Shopping for hydrologically representative connectivity metrics in a humid temperate forested catchment, *Water Resour. Res.*, *46*, W12544, doi:10.1029/2010WR009442.

Asrar, G., M. Fuchs, E. T. Kanemasu, and J. L. Hatfield (1984), Estimating absorbed photosynthetic radiation and leaf-area index from spectral reflectance in wheat, *Agron. J.*, *76*, 300–306.

Asrar, G., R. B. Myneni, and B. J. Choudhury (1992), Spatial heterogeneity in vegetation canopies and remote-sensing of absorbed photosynthetically active radiation—A modeling study, *Remote Sens. Environ.*, *41*, 85–103.

Band, L. E., P. Patterson, R. Nemani, and S. W. Running (1993), Forest ecosystem processes at the watershed scale: Incorporating hillslope hydrology, *Agric. For. Meteorol.*, *63*, 93–126.

Band, L. E., T. Hwang, T. C. Hales, J. Vose, and C. Ford (2012), Ecosystem processes at the watershed scale: Mapping and modeling ecohydrological

controls of landslides, *Geomorphology*, *137*, 159–167, doi:10.1016/j.geomorph.2011.06.025.
Beers, T. W., P. E. Dress, and L. C. Wensel (1966), Aspect transformation in site productivity research, *J. For.*, *64*, 691–692.
Beven, K., and A. Binley (1992), The future of distributed models: Model calibration and uncertainty prediction, *Hydrol. Processes*, *6*, 279–298.
Beven, K., and J. Freer (2001), A dynamic TOPMODEL, *Hydrol. Processes*, *15*, 1993–2011.
Beven, K., and M. Kirkby (1979), A physically-based variable contributing area model of basin hydrology, *Hydrol. Sci. Bull.*, *24*, 43–69.
Bolstad, P. V., W. Swank, and J. Vose (1998a), Predicting southern Appalachian overstory vegetation with digital terrain data, *Landscape Ecol.*, *13*, 271–283, doi:10.1023/A:1008060508762.
Bolstad, P. V., L. Swift, F. Collins, and J. Regniere (1998b), Measured and predicted air temperatures at basin to regional scales in the southern Appalachian mountains, *Agric. For. Meteorol.*, *91*, 161–176.
Bolstad, P. V., J. M. Vose, and S. G. McNulty (2001), Forest productivity, leaf area, and terrain in southern Appalachian deciduous forests, *For. Sci.*, *47*, 419–427.
Bond, B. J., J. A. Jones, G. Moore, N. Phillips, D. Post, and J. J. McDonnell (2002), The zone of vegetation influence on baseflow revealed by diet patterns of streamflow and vegetation water use in a headwater basin, *Hydrol. Processes*, *16*, 1671–1677, doi:10.1002/hyp.5022.
Bracken, L. J., and J. Croke (2007), The concept of hydrological connectivity and its contribution to understanding runoff-dominated geomorphic systems, *Hydrol. Processes*, *21*, 1749–1763, doi:10.1002/hyp.6313.
Brooks, J. R., H. R. Barnard, R. Coulombe, and J. J. McDonnell (2010), Ecohydrologic separation of water between trees and streams in a Mediterranean climate, *Nat. Geosci.*, *3*, 100–104, doi:10.1038/NGEO722.
Brooks, P. D., P. A. Troch, M. Durcik, E. Gallo, and M. Schlegel (2011), Quantifying regional scale ecosystem response to changes in precipitation: Not all rain is created equal, *Water Resour. Res.*, *47*, W00J08, doi:10.1029/2010WR009762.
Broxton, P. D., P. A. Troch, and S. W. Lyon (2009), On the role of aspect to quantify water transit times in small mountainous catchments, *Water Resour. Res.*, *45*, W08427, doi:10.1029/2008WR007438.
Brutsaert, W., and J. P. Lopez (1998), Basin-scale geohydrologic drought flow features of riparian aquifers in the Southern Great Plains, *Water Resour. Res.*, *34*, 233–240, doi:10.1029/97WR03068.
Brutsaert, W., and J. L. Nieber (1977), Regionalized drought flow hydrographs from a mature glaciated plateau, *Water Resour. Res.*, *13*, 637–644, doi:10.1029/WR013i003p00637.
Burgess, S. S. O., and T. E. Dawson (2008), Using branch and basal trunk sap flow measurements to estimate whole-plant water capacitance: A caution, *Plant Soil*, *305*, 5–13, doi:10.1007/s11104-007-9378-2.
Chen, J. M., and T. A. Black (1992), Defining leaf-area index for non-flat leaves, *Plant Cell Environ.*, *15*, 421–429.
Clark, J. S., D. M. Bell, M. H. Hersh, and L. Nichols (2011), Climate change vulnerability of forest biodiversity: Climate and competition tracking of demographic rates, *Global Change Biol.*, *17*, 1834–1849, doi:10.1111/j.1365-2486.2010.02380.x.
Day, F. P., and C. D. Monk (1974), Vegetation patterns on a southern Appalachian watershed, *Ecology*, *55*, 1064–1074.
Day, F. P., D. L. Philips, and C. D. Monk (1988), Forest communities and patterns, in *Forest Hydrology and Ecology at Coweeta*, edited by W. T. Swank and D. A. Crossley Jr., pp. 141–149, Springer, New York.
Detty, J. M., and K. J. McGuire (2010), Topographic controls on shallow groundwater dynamics: Implications of hydrologic connectivity between hillslopes and riparian zones in a till mantled catchment, *Hydrol. Processes*, *24*, 2222–2236, doi:10.1002/hyp.7656.
Ducharne, A., R. D. Koster, M. J. Suarez, M. Stieglitz, and P. Kumar (2000), A catchment-based approach to modeling land surface processes in a general circulation model: 2. Parameter estimation and model demonstration, *J. Geophys. Res.*, *105*, 24,823–24,838.
Eberbach, P. L., and G. E. Burrows (2006), The transpiration response by four topographically distributed *Eucalyptus* species, to rainfall occurring during drought in south eastern Australia, *Physiol. Plant.*, *127*, 483–493, doi:10.1111/j.1399-3054.2006.00762.x.
Eckhardt, K. (2005), How to construct recursive digital filters for baseflow separation, *Hydrol. Processes*, *19*, 507–515, doi:10.1002/hyp.5675.
Ewers, B. E., R. Oren, H. S. Kim, G. Bohrer, and C. T. Lai (2007), Effects of hydraulic architecture and spatial variation in light on mean stomatal conductance of tree branches and crowns, *Plant Cell Environ.*, *30*, 483–496, doi:10.1111/j.1365-3040.2007.01636.x.
Ford, C. R., R. M. Hubbard, B. D. Kloeppel, and J. M. Vose (2007), A comparison of sap flux-based evapotranspiration estimates with catchment-scale water balance, *Agric. For. Meteorol.*, *145*, 176–185, doi:10.1016/j.agrformet.2007.04.010.
Freer, J., K. Beven, and B. Ambroise (1996), Bayesian estimation of uncertainty in runoff prediction and the value of data: An application of the GLUE approach, *Water Resour. Res.*, *32*, 2161–2173.
Freer, J., K. Beven, and N. Peters (2004), Multivariate seasonal period model rejection within the generalised likelihood uncertainty estimation procedure, in *Calibration of Watershed Models, Water Sci. Appl.*, vol. 6, edited by Q. Duan et al., pp. 69–87, AGU, Washington, D. C.
Grayson, R. B., A. W. Western, F. H. S. Chiew, and G. Bloschl (1997), Preferred states in spatial soil moisture patterns: Local and nonlocal controls, *Water Resour. Res.*, *33*, 2897–2908.
Hales, T. C., C. R. Ford, T. Hwang, J. M. Vose, and L. E. Band (2009), Topographic and ecologic controls on root reinforcement, *J. Geophys. Res.*, *114*, F03013, doi:10.1029/2008JF001168.
Harman, C. J., M. Sivapalan, and P. Kumar (2009), Power law catchment-scale recessions arising from heterogeneous linear small-scale dynamics, *Water Resour. Res.*, *45*, W09404, doi:10.1029/2008WR007392.
Hewlett, J. D., and A. R. Hibbert (1967), Factors affecting the response of small watersheds to precipitation in humid areas, in *Forest Hydrology*, edited by N. E. Sopper and H. W. Lull, pp. 275–290, Pergamon, New York.
Hirsch, R. M., and E. J. Gilroy (1984), Methods of fitting a straight line to data: Examples in water resources, *Water Resour Bull.*, *20*, 705–711.
Hopp, L., and J. J. McDonnell (2009), Connectivity at the hillslope scale: Identifying interactions between storm size, bedrock permeability, slope angle and soil depth, *J. Hydrol.*, *376*, 378–391, doi:10.1016/j.jhydrol.2009.07.047.
Horton, R. E. (1933), The role of infiltration in the hydrologic cycle, *Eos Trans. AGU*, *14*, 446–460.
Hwang, T., L. E. Band, and T. C. Hales (2009), Ecosystem processes at the watershed scale: Extending optimality theory from plot to catchment, *Water Resour. Res.*, *45*, W11425, doi:10.1029/2009WR007775.
Hwang, T., C. Song, J. M. Vose, and L. E. Band (2011), Topography-mediated controls on local vegetation phenology estimated from MODIS vegetation index, *Landscape Ecol.*, *26*, 541–556, doi:10.1007/s10980-011-9580-8.
Istanbulluoglu, E., O. Yetemen, E. R. Vivoni, H. A. Gutierrez-Jurado, and R. L. Bras (2008), Eco-geomorphic implications of hillslope aspect: Inferences from analysis of landscape morphology in central New Mexico, *Geophys. Res. Lett.*, *35*, L14403, doi:10.1029/2008GL034477.
Ivanov, V. Y., R. L. Bras, and E. R. Vivoni (2008), Vegetation-hydrology dynamics in complex terrain of semiarid areas: 2. Energy-water controls of vegetation spatiotemporal dynamics and topographic niches of favorability, *Water Resour. Res.*, *44*, W03430, doi:10.1029/2006WR005595.
James, A. L., and N. T. Roulet (2007), Investigating hydrologic connectivity and its association with threshold change in runoff response in a temperate forested watershed, *Hydrol. Processes*, *21*, 3391–3408, doi:10.1002/hyp.6554.
Jencso, K. G., B. L. McGlynn, M. N. Gooseff, S. M. Wondzell, K. E. Bencala, and L. A. Marshall (2009), Hydrologic connectivity between landscapes and streams: Transferring reach-and plot-scale understanding to the catchment scale, *Water Resour. Res.*, *45*, W04428, doi:10.1029/2008WR007225.
Kokkonen, T. S., A. J. Jakeman, P. C. Young, and H. J. Koivusalo (2003), Predicting daily flows in ungauged catchments: Model regionalization from catchment descriptors at the Coweeta Hydrologic Laboratory, North Carolina, *Hydrol. Processes*, *17*, 2219–2238.
Law, B. E., et al. (2002), Environmental controls over carbon dioxide and water vapor exchange of terrestrial vegetation, *Agric. For. Meteorol.*, *113*, 97–120.
Lim, K. J., B. A. Engel, Z. X. Tang, J. Choi, K. S. Kim, S. Muthukrishnan, and D. Tripathy (2005), Automated Web GIS based hydrograph analysis tool, WHAT, *J. Am. Water Resour. Assoc.*, *41*, 1407–1416.
Lindsay, J. B. (2005), The Terrain Analysis System: A tool for hydro-geomorphic applications, *Hydrol. Processes*, *19*, 1123–1130.
Loranty, M. M., D. S. Mackay, B. E. Ewers, E. Traver, and E. L. Kruger (2010), Contribution of competition for light to within-species variability in stomatal conductance, *Water Resour. Res.*, *46*, W05516, doi:10.1029/2009WR008125.
Ludwig, J. A., B. P. Wilcox, D. D. Breshears, D. J. Tongway, and A. C. Imeson (2005), Vegetation patches and runoff-erosion as interacting eco-hydrological processes in semiarid landscapes, *Ecology*, *86*, 288–297.

Mackay, D. S., and L. E. Band (1997), Forest ecosystem processes at the watershed scale: Dynamic coupling of distributed hydrology and canopy growth, *Hydrol. Processes*, *11*, 1197–1217.

Mackay, D. S., B. E. Ewers, M. M. Loranty, and E. L. Kruger (2010), On the representativeness of plot size and location for scaling transpiration from trees to a stand, *J. Geophys. Res.*, *115*, G02016, doi:10.1029/2009JG001092.

McGlynn, B. L., J. J. McDonnell, J. Seibert, and C. Kendall (2004), Scale effects on headwater catchment runoff timing, flow sources, and groundwater-streamflow relations, *Water Resour. Res.*, *40*, W07504, doi:10.1029/2003WR002494.

McGuire, K. J., and J. J. McDonnell (2010), Hydrological connectivity of hillslopes and streams: Characteristic time scales and nonlinearities, *Water Resour. Res.*, *46*, W10543, doi:10.1029/2010WR009341.

McGuire, K. J., J. J. McDonnell, M. Weiler, C. Kendall, B. L. McGlynn, J. M. Welker, and J. Seibert (2005), The role of topography on catchment-scale water residence time, *Water Resour. Res.*, *41*, W05002, doi:10.1029/2004WR003657.

Moore, I. D., G. J. Burch, and D. H. Mackenzie (1988), Topographic effects on the distribution of surface soil-water and the location of ephemeral gullies, *Trans. ASAE*, *31*, 1098–1107.

Myneni, R. B., and D. L. Williams (1994), On the relationship between FAPAR and NDVI, *Remote Sens. Environ.*, *49*, 200–211.

Myneni, R. B., et al. (2002), Global products of vegetation leaf area and fraction absorbed PAR from year one of MODIS data, *Remote Sens. Environ.*, *83*, 214–231.

Nash, J. E., and J. V. Sutcliffe (1970), River flow forecasting through conceptual models part I—A discussion of principles, *J. Hydrol.*, *10*, 282–290.

Pierce, K. B., T. Lookingbill, and D. Urban (2005), A simple method for estimating potential relative radiation (PRR) for landscape-scale vegetation analysis, *Landscape Ecol.*, *20*, 137–147, doi:10.1007/s10980-004-1296-6.

Post, D. A., J. A. Jones, and G. E. Grant (1998), An improved methodology for predicting the daily hydrologic response of ungauged catchments, *Environ. Modell. Software*, *13*, 395–403.

Price, K., C. R. Jackson, and A. J. Parker (2010), Variation of surficial soil hydraulic properties across land uses in the southern Blue Ridge Mountains, North Carolina, USA, *J. Hydrol.*, *383*, 256–268, doi:10.1016/j.jhydrol.2009.12.041.

Pringle, C. (2003), What is hydrologic connectivity and why is it ecologically important?, *Hydrol. Processes*, *17*, 2685–2689, doi:10.1002/hyp.5145.

Rupp, D. E., and J. S. Selker (2006a), Information, artifacts, and noise in $dQ/dt - Q$ recession analysis, *Adv. Water Resour.*, *29*, 154–160, doi:10.1016/j.advwatres.2005.03.019.

Rupp, D. E., and J. S. Selker (2006b), On the use of the Boussinesq equation for interpreting recession hydrographs from sloping aquifers, *Water Resour. Res.*, *42*, W12421, doi:10.1029/2006WR005080.

Sellers, P. J. (1985), Canopy reflectance, photosynthesis and transpiration, *Int. J. Remote Sens.*, *6*, 1335–1372.

Swift, L. W., G. B. Cunningham, and J. E. Douglass (1988), Climatology and hydrology, in *Forest Hydrology and Ecology at Coweeta*, edited by W. T. Swank and D. A. Crossley Jr., pp. 35–55, Springer, New York.

Szilagyi, J., Z. Gribovszki, and P. Kalicz (2007), Estimation of catchment-scale evapotranspiration from baseflow recession data: Numerical model and practical application results, *J. Hydrol.*, *336*, 206–217, doi:10.1016/j.jhydrol.2007.01.004.

Tague, C. L. (2009), Assessing climate change impacts on alpine streamflow and vegetation water use: Mining the linkages with subsurface hydrologic processes, *Hydrol. Processes*, *23*, 1815–1819, doi:10.1002/hyp.7288.

Tague, C. L., and L. E. Band (2004), RHESSys: Regional Hydro-Ecologic Simulation System—An object-oriented approach to spatially distributed modeling of carbon, water, and nutrient cycling, *Earth Interact.*, *8*(19), 1–42, doi:10.1175/1087-3562(2004)8<1:RRHSSO>2.0.CO;2.

Tague, C., and G. E. Grant (2004), A geological framework for interpreting the low-flow regimes of Cascade streams, Willamette River Basin, Oregon, *Water Resour. Res.*, *40*, W04303, doi:10.1029/2003WR002629.

Tarboton, D. G. (1997), A new method for the determination of flow directions and upslope areas in grid digital elevation models, *Water Resour. Res.*, *33*, 309–319.

Tetzlaff, D., J. Seibert, K. J. McGuire, H. Laudon, D. A. Burn, S. M. Dunn, and C. Soulsby (2009), How does landscape structure influence catchment transit time across different geomorphic provinces?, *Hydrol. Processes*, *23*, 945–953, doi:10.1002/hyp.7240.

Tetzlaff, D., C. Soulsby, and C. Birkel (2010), Hydrological connectivity and microbiological fluxes in montane catchments: The role of seasonality and climatic variability, *Hydrol. Processes*, *24*, 1231–1235, doi:10.1002/hyp.7680.

Thompson, S. E., C. J. Harman, P. A. Troch, P. D. Brooks, and M. Sivapalan (2011), Spatial scale dependence of ecohydrologically mediated water balance partitioning: A synthesis framework for catchment ecohydrology, *Water Resour. Res.*, *47*, W00J03, doi:10.1029/2010WR009998.

Troch, P. A., G. F. Martinez, V. R. N. Pauwels, M. Durcik, M. Sivapalan, C. Harman, P. D. Brooks, H. Gupta, and T. Huxman (2009), Climate and vegetation water use efficiency at catchment scales, *Hydrol. Processes*, *23*, 2409–2414, doi:10.1002/hyp.7358.

Voepel, H., B. Ruddell, R. Schumer, P. A. Troch, P. D. Brooks, A. Neal, M. Durcik, and M. Sivapalan (2011), Quantifying the role of climate and landscape characteristics on hydrologic partitioning and vegetation response, *Water Resour. Res.*, *47*, W00J09, doi:10.1029/2010WR009944.

Vose, J. M., and W. T. Swank (1990), Assessing seasonal leaf-area dynamics and vertical leaf-area distribution in eastern white pine (*Pinus strobus* L.) with a portable light meter, *Tree Physiol.*, *7*, 125–134.

Vose, J. M., P. M. Dougherty, J. N. Long, F. W. Smith, H. L. Gholz, and P. J. Curran (1994), Factors influencing the amount and distribution of leaf area of pine stands, *Ecol. Bull.*, *43*, 102–114.

Wagener, T., and H. S. Wheater (2006), Parameter estimation and regionalization for continuous rainfall-runoff models including uncertainty, *J. Hydrol.*, *320*, 132–154, doi:10.1016/j.jhydrol.2005.07.015.

Webb, W., S. Szarek, W. Lauenroth, R. Kinerson, and M. Smith (1978), Primary productivity and water-use in native forest, grassland, and desert ecosystems, *Ecology*, *59*, 1239–1247, doi:10.2307/1938237.

Western, A. W., R. B. Grayson, G. Bloschl, G. R. Willgoose, and T. A. McMahon (1999), Observed spatial organization of soil moisture and its relation to terrain indices, *Water Resour. Res.*, *35*, 797–810.

Western, A. W., G. Bloschl, and R. B. Grayson (2001), Toward capturing hydrologically significant connectivity in spatial patterns, *Water Resour. Res.*, *37*, 83–97.

Whittaker, R. H. (1956), Vegetation of the Great Smoky Mountains, *Ecol. Monogr.*, *26*, 1–69.

Wigmosta, M. S., L. W. Vail, and D. P. Lettenmaier (1994), A distributed hydrology-vegetation model for complex terrain, *Water Resour. Res.*, *30*, 1665–1679.

Woods, R. A., and M. Sivapalan (1997), A connection between topographically driven runoff generation and channel network structure, *Water Resour. Res.*, *33*, 2939–2950.

Yeakley, J. A., W. T. Swank, L. W. Swift, G. M. Hornberger, and H. H. Shugart (1998), Soil moisture gradients and controls on a southern Appalachian hillslope from drought through recharge, *Hydrol. Earth Syst. Sci.*, *2*, 41–49.